Q. J. R. Meteorol. Soc. (2001), **127**, pp. 559–577

Southern hemisphere winter ozone fluctuations

By P. K. VIGLIAROLO[1]*, C. S. VERA[2] and S. B. DIAZ[1]
[1]*CADIC-CONICET, Argentina*
[2]*CIMA-CONICET, University of Buenos Aires, Argentina*

(Received 10 March 2000; revised 14 August 2000)

SUMMARY

In this paper the relationship between ozone and atmospheric variability is explored over the southern hemisphere during the austral winter season, with special emphasis on synoptic transient fluctuations.

The analysis of ozone tracks (or high-frequency ozone variability) shows that they have a significant correspondence with storm tracks at middle and high latitudes. Moreover, ozone tracks maximize over the Indian Ocean slightly downstream of the storm-track maximum, while over the Pacific region both ozone and storm tracks show decreased amplitudes.

In particular, over southern South America (a region of climatological winter ozone minima and moderate to high ozone variability) the leading winter synoptic-scale variability mode was identified through a rotated extended empirical orthogonal function analysis applied to the meridional-wind perturbation at 300 hPa. The resulting mode is characterized by a baroclinic wave travelling eastward along subpolar latitudes, which maximizes near the tropopause level. Composite ozone fields based on this mode confirm, from a statistical point of view, the classical relationship between ridges (troughs) and minimum (maximum) ozone content. Furthermore, it is shown that dynamical processes in the upper troposphere and lower stratosphere associated with subpolar waves are responsible for the observed ozone distribution. This happens due to the barotropic equivalent vertical structure of the wave, together with the fact that ozone partial pressure maximizes near the level where the waves attain maximum amplitudes.

KEYWORDS: Baroclinic waves Ozone tracks Ozone–weather relationship Storm tracks Synoptic variability

1. INTRODUCTION

Transient wave activity in the tropopause and/or lower stratosphere strongly influences total ozone columnar content through both vertical and horizontal advection, although ozone partial pressure is a maximum in the lower stratosphere at around 20–25 km (Andrews *et al.* 1987; Orsolini *et al.* 1998). Some foregoing papers have focused on studying regions of high-frequency ozone variability, and relating them to atmospheric variability. Schubert and Munteanu (1988) showed that total ozone and tropopause pressure are remarkably correlated in middle latitudes of both hemispheres all the year round on synoptic time-scales (i.e. zonal wave numbers larger than five and temporal scales shorter than ten days). In fact, the areas of highest correlations seem to be associated with the storm-track regions (or areas of maximum high-frequency atmospheric activity). However, the authors mentioned that the nature of the correspondence between high correlation and high ozone variability is not yet clear. Allen and Reck (1997) found that the day-to-day differences of total ozone induced by medium-scale waves (i.e. zonal wave numbers 4–7) exhibit larger values than those fluctuations induced by planetary waves (zonal wave numbers 1–3). Orsolini *et al.* (1998) examined by band-pass filtering, storm-track patterns in northern hemisphere (NH) total ozone (which they refer to as ozone tracks), and they found a strong relationship between ozone and storm tracks. Furthermore, the North Atlantic ozone track is stronger than the North Pacific one, probably due to intense ozone mini-hole events in the Atlantic sector.

It is well known that high-frequency variability explains a large perecentage of total transient ozone variance of the southern hemisphere (SH; Trenberth 1991). The SH storm track is mostly zonally oriented along 50°S during all seasons, and strongly correlates with the regions of maximum mean baroclinicity (Berbery and Vera 1996).

* Corresponding author: CADIC, Ruta 3 y Cap.Mutto s/n, CC92, 9410, Ushuaia, Tierra del Fuego, Argentina.
e-mail: paulav@ciudad.com.ar

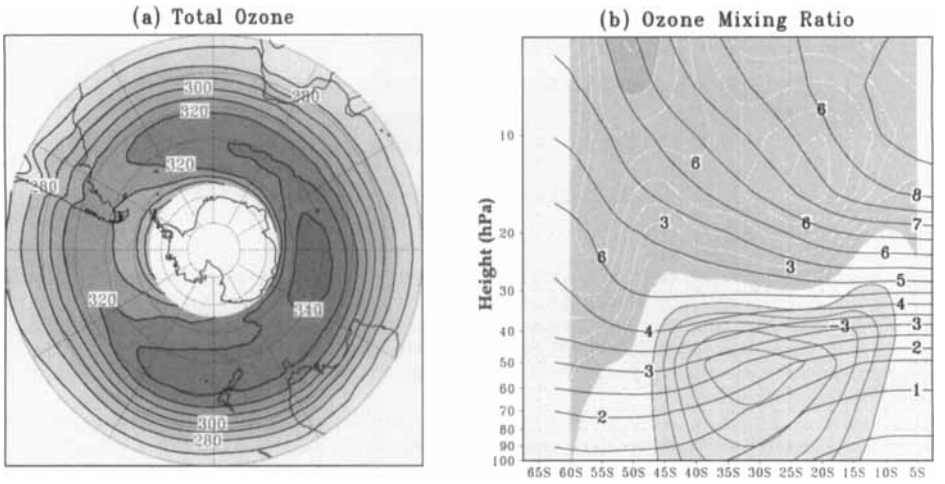

Figure 1. (a) Mean total ozone distribution for the southern hemisphere winter months of 1983–88; the contour interval is 10 DU. (b) Vertical cross-section of zonal mean ozone mixing ratio from a solar backscatter ultraviolet instrument, for the same period, displayed every 0.5 parts per million by volume (p.p.m.v.). Light (heavy) shades represent positive (negative) mean ozone meridional gradient; the contour interval is 1×10^{-7} p.p.m.v. m^{-1}, and the zero contour has been omitted. Note that the vertical cross-section includes values above 100 hPa only.

However, besides the results of Schubert and Munteanu (1988) and Allen and Reck (1997), the linkage between ozone and storm tracks over the SH has not yet been extensively explored. Thus, the geographical distribution of ozone variability in the SH winter and its relationship with upper-tropospheric fluctuations on synoptic time-scales is also studied in this paper.

The association between ozone fluctuations and weather systems has long been investigated but almost entirely through studies of individual cases (e.g. Orlanski *et al.* 1989; McKenna *et al.* 1989; Rood *et al.* 1992; Orsolini *et al.* 1995, etc.). Mote *et al.* (1991) examined the climatological signatures of baroclinic wave trains on total ozone fields for the NH winter by means of regression techniques. But, to the authors' knowledge, there is a lack of research about the statistical characteristics of the relationship between baroclinic waves and ozone variations in the SH. Therefore, in this paper this relationship is addressed over southern South America (SSA), a region of climatological low ozone amounts (Fig. 1(a)) and moderate to high ozone variability (Fig. 3(c) and (d)).

This paper is organized as follows. Section 2 describes the dataset used, whilst in section 3 the structure of SH winter stationary waves is examined, with emphasis on describing zonal asymmetries of mean fields. SH transient atmospheric activity and ozone fluctuations within the winter season are explored in section 4, focusing on the relationship between ozone tracks and storm tracks. Section 5 includes the study of leading modes of synoptic-scale variability over SSA and related signatures in ozone fields. Finally, the conclusions are outlined in section 6.

2. Data

The dataset is based on six winters (1983–88) of the European Centre for Medium-Range Weather Forecasts daily 1200 UTC analyses, on a regular 2.5° latitude by 2.5° longitude grid, and for the vertical levels of 1000, 850, 700, 500, 300, 200 and 100 hPa. Throughout the paper, winter relates to the austral season and is defined as the period

from 1 June to 31 August. The meteorological variables used in this paper include: zonal wind (u), meridional wind (v), pressure velocity (ω), temperature (T) and geopotential height (z). Trenberth (1992) has discussed both the quality of the dataset and the changes in the assimilation systems.

The daily Total Ozone Mapping Spectrometer (TOMS) gridded dataset (version 7), on board the Nimbus 7 satellite (McPeters and Beach 1996) was also used in this study. The horizontal resolution of the data is 1° in latitude and 1.25° in longitude. TOMS data require backscattered sunlight for their measurement, thus the polar night precludes inclusion of latitudes higher than 65°S (Stanford *et al.* 1995). The winter distribution of SH mean total ozone (Fig. 1(a)) displays a ring-like structure, with maximum values along mid latitudes (40°–60°S), decreasing polewards and equatorwards.

The Brewer–Dobson circulation provides the mechanism through which ozone is transported from the tropical source region to the middle and high latitudes where high ozone values are observed. While the SH mid-latitude ozone maximum is due to downward velocities associated with the descending branch of the Brewer–Dobson circulation that maximizes over the edge of the polar vortex, the total column ozone minimum over Antarctica is the result of the isolation from mid-latitude air provided by the same vortex. Moreover, the strength of the polar vortex is directly related (by thermal-wind balance) to the low temperatures required for ozone-depleting heterogeneous chemistry (Wardle *et al.* 1997). Also, there is evidence that air in the centre of the polar vortex has come from the mesosphere, well above the ozone maximum, thus one would expect ozone values to be lower there than near the vortex edge (Fisher *et al.* 1993; Wardle *et al.* 1997).

Nevertheless, longitudinal differences at the latitudes of the maximum are noticeable. While values above 340 DU are found over the south-eastern Indian Ocean (55°S, 100°E), over the south-eastern Pacific Ocean and SSA values drop to about 300 DU. Additionally, for this region a high-latitude ozone minimum extends over the Antarctica Peninsula and reaches SSA. According to Randel and Newman (1998), during spring SSA constitutes a region of preferred wave-breaking, linked to the displacement of the South Polar vortex towards this region and in close association with the presence of the stationary planetary wave number one.

The SH zonal mean ozone mixing ratio (Fig. 1(b)) was calculated from the monthly Nimbus 7 Solar Backscatter Ultraviolet (SBUV) data (details of the instrument and information on data retrievals are in McPeters *et al.* (1994), Randel and Wu (1995) and references therein). Each monthly profile is given in zones averaged over 5°latitude and at standard pressure levels from 100 to 5 hPa. From Fig. 1(b) it is evident that the ozone mixing ratio increases with height and equatorwards, reaching a maximum over tropical latitudes at around 10 hPa. In the lower stratosphere up to 30 hPa, the ozone maximum is found over middle latitudes around 45–55°S, demonstrated by the change in sign of the horizontal gradient of ozone mixing ratios. From 30 hPa and upwards, the horizontal positive gradient of ozone increases, exhibiting a conspicuous maximum above 10 hPa and a weaker maximum between 20 and 10 hPa at subtropical latitudes. South of 50°S, ozone mixing ratios show little variation with height.

3. Stationary waves

In this section, the characteristics of the stationary waves are analysed in order to highlight the longitudinal differences of mean total ozone distribution at SH high-latitudes during winter (Fig. 1(a)). Stationary waves are defined as the zonal asymmetries of the mean fields (calculated as the difference between the mean winter field and

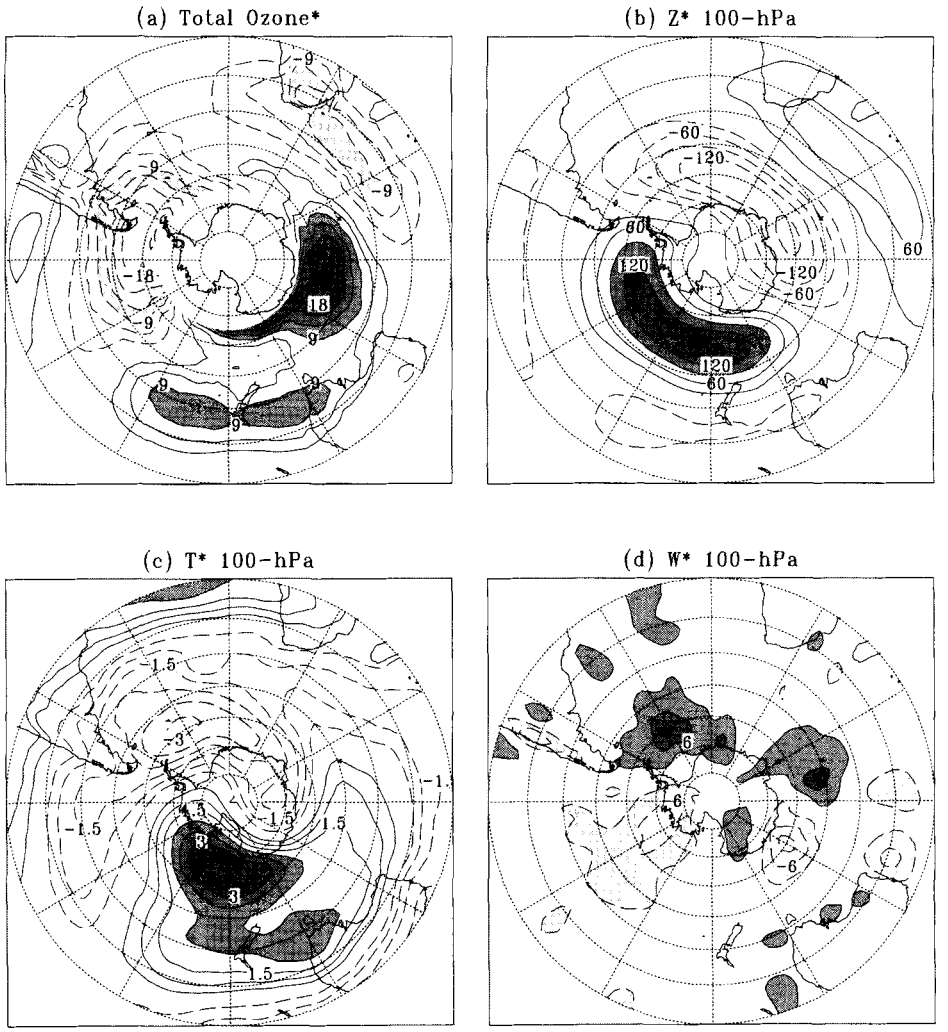

Figure 2. Zonal asymmetries of the mean fields for: (a) total ozone; and 100 hPa: (b) geopotential height, (c) temperature, and (d) vertical velocity. Contour intervals are: (a) 3 DU, (b) 30 m, (c) 0.5 K and (d) 3×10^{-3} Pa s^{-1}. All zero contours have been omitted; maxima and minima are shaded.

the corresponding zonal mean) and are denoted by asterisks. The total ozone stationary component (Fig. 2(a)) suggests a predominance of wave number one at high latitudes, reaching peak values of −21 DU over the southern tip of South America, and 18 DU near 55°S, 90°E. Wirth (1993) found that during austral spring ozone stationary anomalies are about three times as strong and displaced a little polewards and eastwards. In addition, during winter SH ozone anomalies as large as 9 DU are found at around 30°S from 140°E eastwards to 150°W, and also to the south-east of South Africa but with opposite sign.

The lower-stratospheric geopotential height stationary field (Fig. 2(b)) resembles, over mid and high latitudes, wave number one structure (in agreement with Randel (1992) and Randel and Newman (1998)), with anomalies exceeding 120 m in magnitude along the 60°S latitude circle. Moreover, wave nodes are located slightly to the east of the ozone maximum (over the south-eastern Indian Ocean) and ozone minimum (over

SSA). The stationary component of the atmospheric waves undergoes a marked annual cycle, with a minimum in midwinter and a maximum during September and October (Randel and Newman 1998). Also, as has already been noted in preceding paragraphs, the ozone stationary wave largely increases during spring relative to the winter season (Randel and Wu 1995).

The 100 hPa temperature stationary-wave pattern displays a cold centre over 60°S 30°W of −3 K and a warm centre near the date line and over 65°S exceeding 3.5 K (Fig. 2(c)). Each centre stretches out to higher latitudes over the southern Indian and Pacific Oceans. The negative (positive) temperature extreme is displaced to the west with respect to the negative (positive) geopotential height centre (Fig. 2(b)). A secondary warm centre extends from south-eastern Australia towards 160°E.

Figure 2(d) shows a stationary velocity pattern at 100 hPa. In general, ω^* is a maximum at high latitudes poleward of 50°S, with values as large as -0.006 Pa s^{-1} over the Pacific Ocean, and velocities of about 0.006 Pa s^{-1} over the Atlantic and Indian Oceans. In addition, both upward and downward motion centres are located either side of the Antarctica Peninsula where the stationary ozone anomalies are at minima (Fig. 2(a)). A similar dipole pattern is also observed across 90°E longitude, close to the location of maximum ozone stationary component.

Over middle and high latitudes, Wirth (1993) and Kurzeja (1984) apply the stationary ozone continuity equation in order to understand the origin of ozone zonal asymmetries of the SH spring and NH winter, respectively. They conclude that meridional and vertical advection terms contribute equally to ozone stationary-pattern maintenance. In this sense, it seems that a similar situation is taking place during SH winter over middle and high latitudes (see Fig. 2), although the anomaly of the ozone net source may also play an important role and thus should also be taken into account. This term is known to be small over the lower stratosphere on monthly time means (Solomon and Garcia 1985; Wirth 1993; Hood *et al.* 1997; among others) but this may no longer hold on a seasonal basis. Still, detailed numerical simulations need to be performed to address quantitatively the relative relevance of the mechanisms that are responsible for the observed ozone asymmetries.

At subtropical latitudes, ozone stationary patterns are related to geopotential height and temperature anomalies via the *tropopause effect* (Stephenson and Royer 1995; Stanford *et al.* 1995; Ambrizzi *et al.* 1998; among others), which may be viewed as a strong modulation of the total ozone column by upper-tropospheric disturbances. Using the ozone continuity equation and considering adiabatic processes, Hood *et al.* (1997) show that for the lower stratosphere, the (positive) zonal gradient of ozone mixing ratio is related to both the (positive) zonal gradient of temperature anomaly and the (negative) zonal gradient of geopotential height anomaly. This relationship is consistent with the tropopause-effect mentioned above, in particular over the New Zealand high-ozone region, where a cyclonic stationary centre (Fig. 2(b)) is associated with a depressed tropopause (not shown) and positive lower-stratospheric temperature anomalies (Fig. 2(c)). Conversely, over southern South Africa and eastwards, negative ozone anomalies are related to an uplift of ozone mixing ratio surfaces due to the presence of a positive stationary geopotential height anomaly, whereas relatively weak negative temperature anomalies are also evident.

4. Storm tracks and ozone tracks

In this section the SH winter transient activity and its relationship with ozone fluctuations are explored. Figure 3(a) displays the standard deviation of the 300 hPa

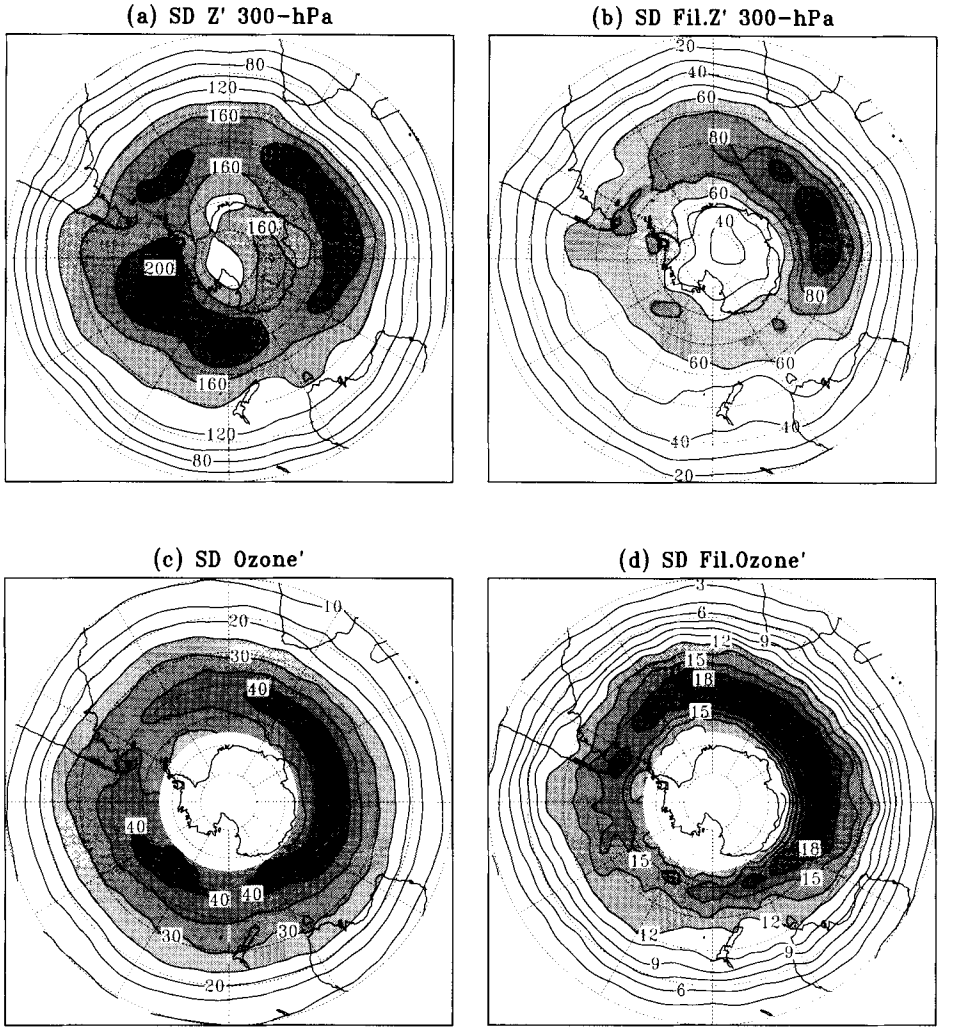

Figure 3. Winter standard deviations of the perturbations of unfiltered (a) 300 hPa geopotential height, and (c) total ozone; and high-frequency band-pass filtered (b) 300 hPa geopotential height, and (d) total ozone. Contour intervals are (a) 20 m, (b) 10 m, (c) 5 DU and (d) 1.5 DU.

geopotential height perturbations after removing the seasonal cycle and the interannual variability, as defined in section 2. Maximum values are found within the 45–70°S latitude band, with values exceeding 200 m over the southern Pacific and central southern Indian Ocean, while a secondary maximum is also noticeable east of SSA. In addition, it was found that throughout the troposphere and lower stratosphere, geopotential height standard deviation centres are closely linked to regions of enhanced meridional heat fluxes (not shown), indicating that baroclinic processes are dominant at subpolar latitudes (Trenberth 1991; Berbery and Vera 1996).

The standard deviation of the temporal ozone perturbations was calculated in a similar way (Fig. 3(c)), and the following features are evident. (a) A band of large values of standard deviation extends along 55°S from south of Africa to south of Australia, with a maximum located over the Indian Ocean between 60° and 100°E upstream of the mean total-ozone maximum (Fig. 1(a)). (b) A secondary maximum is observed over

the Pacific Ocean between 115 and 170°W, downstream and poleward of the band of largest values of mean total ozone located at around 45°S. (c) Minimum values of ozone standard deviation and of mean total ozone are observed at the same latitude south-east of South America and over the south-western Atlantic Ocean.

Remarkable coherence between ozone and geopotential height standard deviation distributions (Fig. 3(a) and (c)) is noticed along the latitude belt of maximum areas, especially over the Indian and Central Pacific basins. This result agrees with those obtained by other authors (Schubert and Munteanu 1988; Salby and Callahan 1993; Allen and Reck 1997; among others) about the main role of transients on ozone variability.

A widely used measure of high-frequency wave activity is the standard deviation of band-pass filtered variables (Blackmon *et al.* 1984; Trenberth 1991; among others). In that sense a 21-point band-pass filter was applied to the data in order to retain the short time-scale variability between 2.5- and 6-day periods (Berbery and Vera 1996). The winter storm track, defined by the standard deviation of the filtered geopotential height at 300 hPa (Fig. 3(b)), displays values of about one-half relative to those defined by the unfiltered geopotential height standard deviation (Fig. 3(a)). Both exhibit a maximum over the Indian Ocean, but the secondary maximum over the central South Pacific Ocean present in the standard deviation of the unfiltered data is not evident in the filtered field, and thus it must be associated with the activity of lower-frequency fluctuations. It is worth noting that standard deviation of the filtered geopotential height at 500 hPa essentially exhibit the same features as those shown in Fig. 3(b).

Figure 3(d) shows the distribution of the SH ozone track during winter, calculated as the standard deviation of the filtered ozone perturbations. As was found for the storm track, the SH ozone-track pattern agrees with the ozone standard deviation (Fig. 3(c)), but with values that are around 45% of the latter over mid to high latitudes of the Atlantic and Indian Oceans. On the other hand, the ozone track minimizes over the South Pacific Ocean where the ozone standard deviation maximizes. This result indicates that ozone variability there is due to lower-frequency atmospheric fluctuations, as was previously mentioned for the geopotential height variability over than region.

A comparison of Fig. 3(d) and (b) shows that ozone-track and storm-track regions are nearly coincident, indicating the primary role of upper-tropospheric disturbances in producing high-frequency ozone fluctuations. The filtered ozone standard deviation maximizes over the Indian Ocean slightly downstream of the storm-track maximum, particularly between 60 and 120°E. In addition, the relatively weak Pacific storm-track region corresponds to minimum ozone filtered standard deviation values. It is interesting to note that over SSA, where the storm track begins, a relative maximum of ozone track of 16.5 DU occurs. These results are consistent with those of Orsolini *et al.* (1998) for the NH winter season, which show a good spatial correspondence between ozone tracks and storm tracks; the latter being calculated using band-pass filtered geopotential height fields at 500 hPa. They noticed that in the NH ozone usually peaks over the storm-track entrance regions, where the meridional ozone gradient is also strongest in the lower stratosphere.

5. Winter synoptic-scale waves and ozone variations

Berbery and Vera (1996) show that synoptic-scale waves at SH subpolar latitudes during austral winter exhibit significant longitudinal differences in wave periods and wavelengths. Therefore, in agreement with Orsolini *et al.* (1998), zonal wave number

decomposition does not seem to be the most appropriate method for identifying propagating synoptic-scale waves. Instead, to represent short time-scale perturbations, we use the 300 hPa meridional wind perturbation (v') time series, which is defined as the difference between each daily value and the time mean of the corresponding winter season; this removes any interannual variability from the series. Berbery and Vera (1996) have shown that no further data filtering is necessary, as the meridional wind perturbation defined in that way concentrates most of its variability at synoptic scales.

(*a*) *Analysis procedure*

The rotated extended empirical orthogonal function (REEOF) technique was applied to the 300 hPa meridional wind temporal series in order to identify the leading modes of synoptic-scale variability over SSA. A REEOF analysis of four one-day lag units was performed over a domain that extends from 130 to 20°W and 80 to 10°S. The EEOF modes were computed from the correlation matrix. To maximize the local variance within the domain, the EEOF modes were rotated using the Varimax method. The choice of the number of eigenmodes to be rotated follows O'Lenic and Livesey (1988). Because the 300 hPa level was chosen, as for the reference time series, the REEOF system should best represent upper-level systems. However, changing the level of reference did not affect any of the results reported here (see also Vera and Vigliarolo 2000).

The first four REEOF modes obtained explain 5%, 4%, 3.8% and 3.6% of the total variance, respectively, where each individual variance is about one-fourth of that obtained from an EOF analysis (Lau and Chan 1985). Modes appear in pairs that have a quadrature phase-shift, thus representing the propagation of the same local wave, and they display the typical horizontal structure of eastward-travelling baroclinic waves (Figs. not shown). While the first pair of modes propagates along subpolar-jet latitudes, the second pair propagates along subtropical-jet latitudes. As one of the main goals of this paper is to diagnose the mid- to high-latitude synoptic-scale waves and associated signatures in the ozone field, the first REEOF was chosen and designated as subpolar mode. Composite maps of the meteorological variables and ozone were constructed to describe subpolar-mode characteristics. Positive (negative) composites refer to the five-day time evolution obtained by averaging daily fields associated with values of REEOF temporal coefficients larger (smaller) than 0.8 (−0.8) times the standard deviation of the series. The statistical significance of the composite fields was checked using a t-test and assuming 100 degrees of freedom at the 5% significance level.

In the following subsections, the structure and temporal evolution of synoptic-scale waves over SSA and related signatures in total ozone fields are studied through the analysis of the first REEOF, or subpolar mode. First, attention is focused on negative composite fields, which are related to the evolution of an anticyclonic perturbation and a transient ozone depression. In subsection (c) positive composite fields (which are associated with a cyclonic perturbation and a travelling ozone maximum) are briefly described, highlighting the main differences from the anticyclonic case.

(*b*) *Negative composites*

The time evolution of the negative composite fields of the 300 hPa meridional wind perturbation is shown in Fig. 4. This pattern corresponds to a localized wave packet that extends from southern Australia towards Africa along mid to high latitudes of the Pacific and Atlantic Oceans. The dominant wave pattern over South America has a length of about 5000 km and an easterly phase velocity of nearly 9 m s^{-1} over the Pacific Ocean, while decreasing eastward to 8 m s^{-1} over the Atlantic Ocean. These results agree with

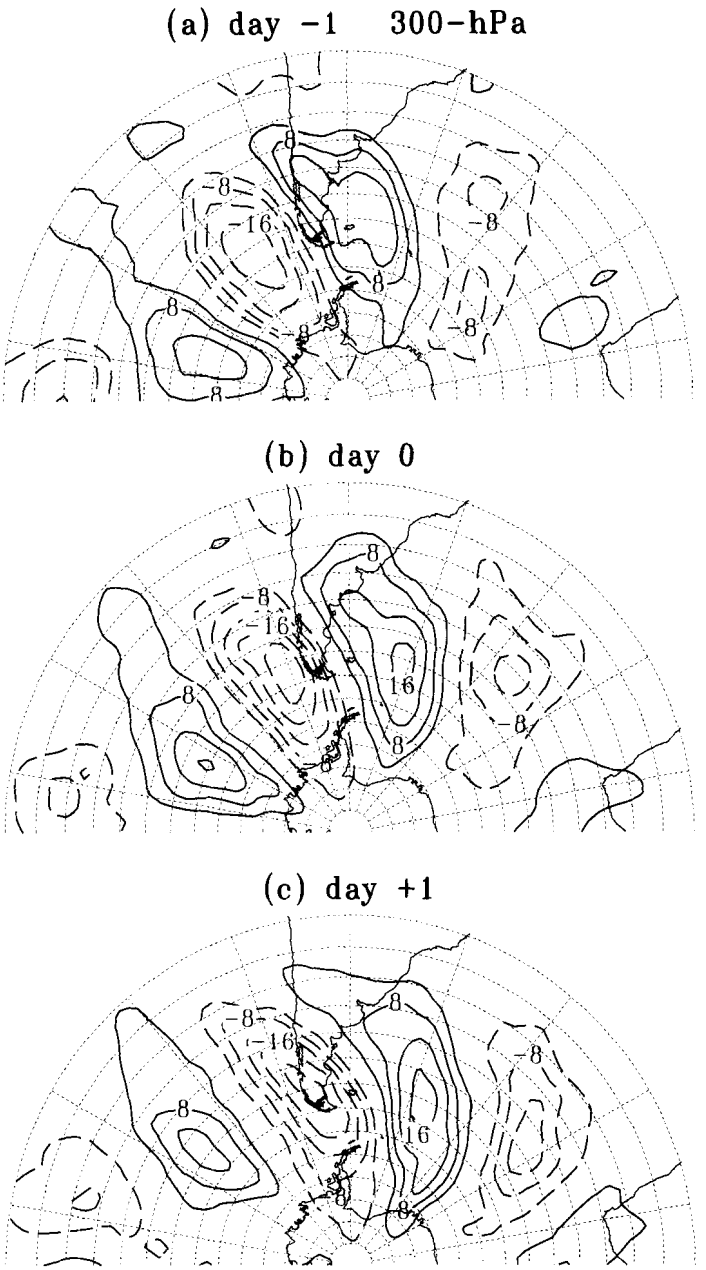

Figure 4. (a)–(c) Subpolar-mode negative composites of meridional wind perturbation at 300 hPa, for days −1, 0 and +1 respectively. The contour interval is 4 m s^{-1} and the zero contours are omitted.

Berbery and Vera (1996), who showed that waves evolving along subpolar latitudes are faster and of a lower wave number compared with those eastward-travelling waves along subtropical latitudes. The temporal evolution from day −1 to day +1 (Fig. 4(a) to (c)) indicates that new centres grow downstream, while decaying centres are seen on the upstream side. Over the Pacific Ocean waves follow a mainly zonal trajectory while, when approaching SSA, they become more meridionally elongated and, once over the

Atlantic, start to propagate equatorwards (Berbery and Vera 1996; Vera and Vigliarolo 2000). By day 0 (Fig. 4(b)) the meridional wind perturbation reaches a maximum of about 20 m s^{-1} off the east Coast of Chile. From day +1 (Fig. 4(c)) to the end of the sequence (not shown), waves start to decay.

Figure 5 depicts the time evolution of the composite fields of total ozone, 300 hPa streamlines and 100 hPa vertical wind perturbation for the first three days of the sequence. From the early stages (Fig. 5(a)), a strong asymmetry in the total ozone field manifests itself, with relatively low ozone contents (below 290 DU) occurring over a wide region of SSA, while high ozone amounts (exceeding 320 DU) are found both over Pacific and Atlantic Oceans. Inspection of total ozone fields associated with the subpolar mode (Fig. 5) confirms the typical relationship between troughs (ridges) and maximum (minimum) ozone content. Ozone reaches a minimum of 270 DU over SSA by day −1 (Fig. 5(b)), which is associated with the transient ridge maximizing between days −1 and 0 over the same region (Fig. 5(b) and (c)). This result agrees with the conceptual framework elaborated by Orlanski *et al.* (1987) that relates the circulation of a typical SH baroclinic wave with the resultant total ozone distribution, considering ozone as a conservative tracer. They conclude that, as in the SH the horizontal ozone mixing-ratio gradient in the lower stratosphere is reversed at mid latitudes (Fig. 1(a)), then the contours of ozone content will be out of phase with those of geopotential height.

Figure 5 shows that upward (downward) motions are observed behind the ridges (troughs), while downward (upward) motions occur to the front. Air at the rear of the anticyclone is advected south-eastward and upward, lifting constant ozone mixing-ratio surfaces. As a consequence, ozone number density decreases within air parcels as they cross the constant-pressure surfaces. On the top of the ridge, vertical velocities become zero and parcels reach their maximum altitude, thus the ozone minimum occurs there. Once downstream, air is advected to the north-east and downward, which leads to ozone enhancement over the trough, as seen over the western Atlantic Ocean by day 0 (Fig. 5(c)).

For some time, the role of the advection processes by atmospheric flow has been recognized in strongly influencing extratropical ozone distribution (Reed 1950; McKenna *et al.* 1989; Vaughan and Price 1991; among others). Schoeberl and Krueger (1983) have successfully modelled the evolution of a transient synoptic depression in the ozone field by means of atmospheric advection, and shown that both horizontal and vertical components produce comparable ozone anomalies. Figure 5 suggests that the upper-tropospheric circulation accounts for the distribution of ozone, in part because of the small vertical tilt of subpolar waves, especially in the upper troposphere and lower stratosphere (as will be shown next). A proposed schematic view of an idealized baroclinic wave and the resulting ozone partial-pressure distribution is shown in Fig. 6.

Figure 7 shows geopotential height (Fig. 7(a)) and temperature (Fig. 7(b)) perturbations at 200 hPa on day −1, that is the time when ozone fluctuations reach a minimum over SSA (Fig. 5(b)). Ozone and geopotential height perturbations are strongly anti-correlated (Fig. 7(a)) in agreement with the findings of Schoeberl and Krueger (1983), Stanford *et al.* (1995) and Hood *et al.* (1997), among others. Ozone perturbation values lower than −20 DU cover the southern portion of South America and adjacent seas, with a minimum of −25 DU located all along the tip of SSA, whilst the geopotential height maximum exceeds 160 m over the same region. Conversely, near 65°S 115°W the ozone perturbation is about 30 DU, in association with geopotential perturbation values of about −160 m. A coupling between lower-stratospheric temperature and ozone perturbations is also evident (Fig. 7(b)), although temperature centres are displaced northwards relative to ozone centres. Typical values of 200 hPa T' of 4.5 K are found over the

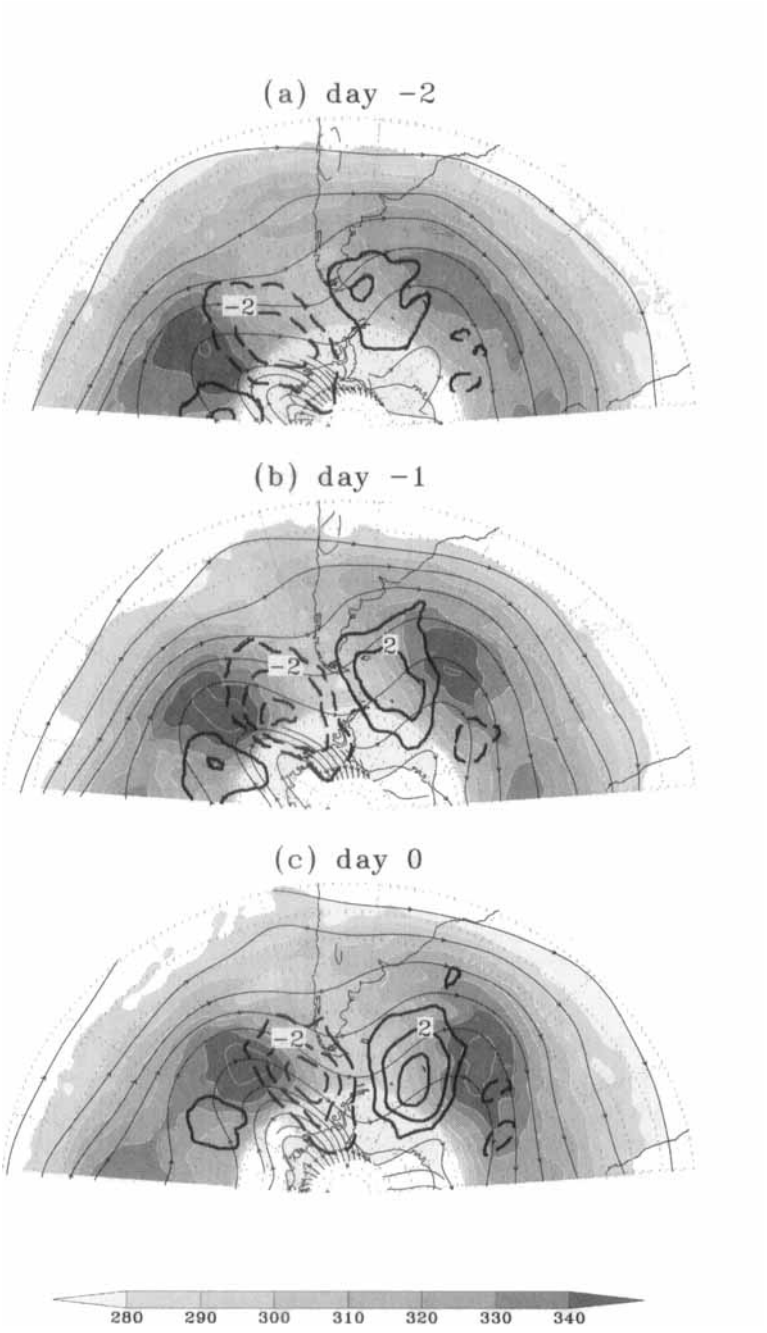

Figure 5. (a)–(c) Subpolar mode negative composites of total ozone (shaded, every 10 DU), streamlines at 300 hPa (light contours) and vertical velocities at 100 hPa (heavy contours every 1×10^{-2} Pa s^{-1}, the zero contour omitted), from day −2 to day 0. Note that negative values (dashed contours) denote ascent, while positive values (continuous contours) correspond to descent.

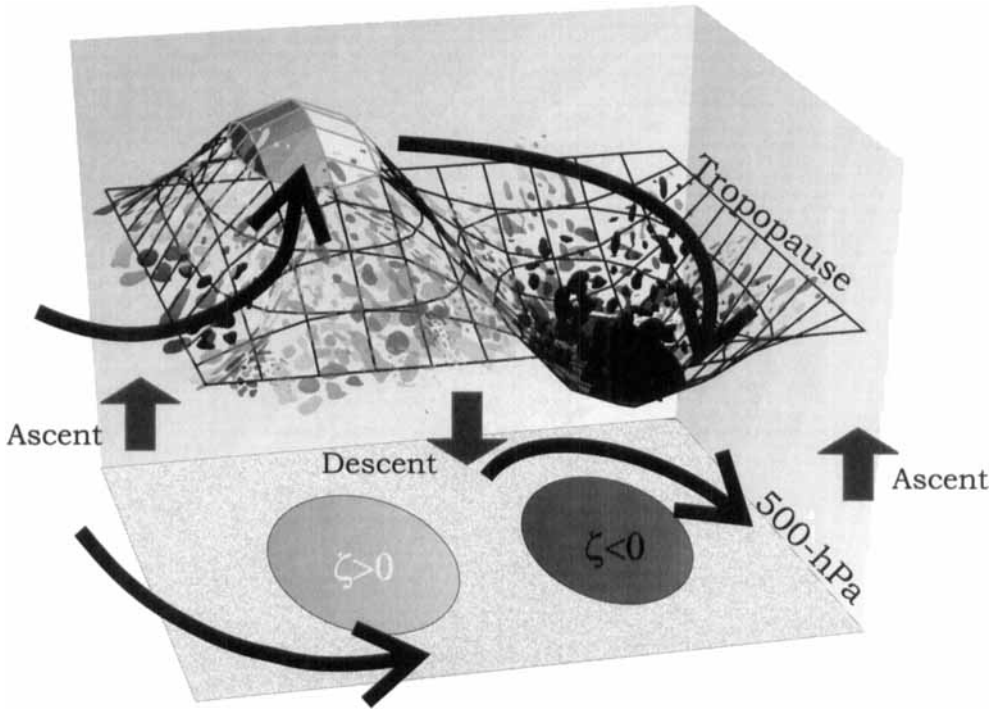

Figure 6. Idealized scheme of a synoptic baroclinic wave and the associated ozone abundance field (denoted by dots). The wave models the tropopause in such a way that the ridge (trough) is associated with a high (low) tropopause. As these waves attain their maximum in the upper troposphere, the ozone layer is deeper where the tropopause is lower and vice versa. Air in the lower stratosphere tends to follow the tropopause, which leads to ascent between trough and ridge and descent between ridge and trough (note that in the southern hemisphere positive relative-vorticity values are associated with ridges and negative ones with troughs). Similarly, the meridional velocity associated with the wave will be polewards to the rear of the ridge and equatorwards to the front. At the same time, the wave evolves to the east as it is embedded in the subpolar jet flow (horizontal motions are projected onto a middle atmospheric level, such as 500 hPa). As a consequence of this three-dimensional structure, ozone tends to accumulate over the trough, while over the ridge ozone content decreases.

Pacific sector and −3 K over the SSA region, thus yielding positive correlation with the ozone perturbation field. Hood *et al.* (1997) show that over time-scales under a month, correlations of both lower-stratospheric temperature and geopotential height with total ozone should be explained in terms of advective ozone transports under adiabatic conditions. For the subpolar mode, the ratios of ozone perturbations to lower-stratospheric z' and T' are of the order of -1 to -1.5 DU dam^{-1} and 6 to 8 DU K^{-1} respectively (each was calculated following the perturbation centres displayed in Fig. 7). These ratios are in qualitative agreement with the results of Hood *et al.* (1997), Newman and Randel (1988) and Randel and Cobb (1994); the last two in respect of ozone–temperature ratios. Furthermore, ratios ranging from 6 to 10 DU K^{-1} of total ozone to lower-stratospheric temperature changes are obtained based on dynamical forcing (Ziemke *et al.* 1997). Consequently, our results indicate that SH subpolar waves constitute an essential dynamical contributor to ozone synoptic-scale changes during winter. Throughout the rest of the time evolution the ratios remain almost constant within the domain (not shown).

Figure 8 describes the vertical structure of the subpolar mode, which agrees well with the results of Lim and Wallace (1991). The vertical distribution of the geopotential height perturbation, averaged between 50 and 55°S (Fig. 8(a)), exhibits maximum

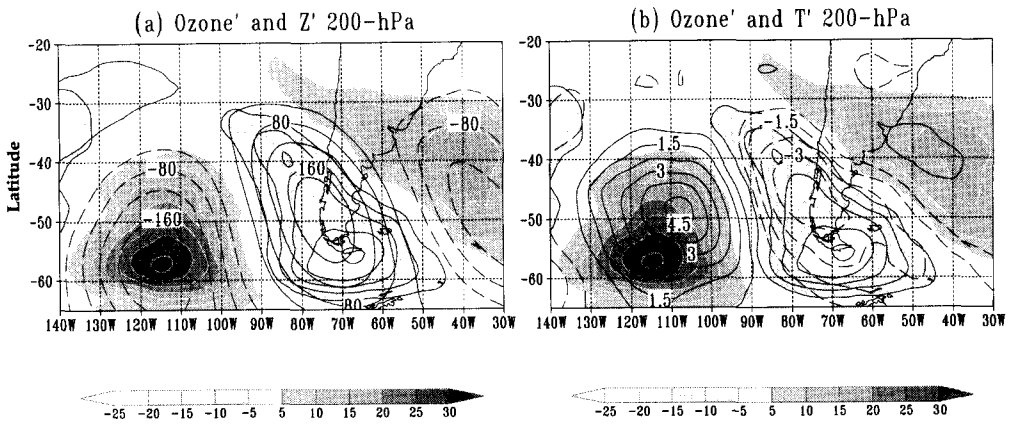

Figure 7. Negative composites of ozone perturbation (shaded every 5 DU) with: (a) 200 hPa geopotential height perturbation (contoured every 40 m), and (b) 200 hPa temperature perturbation (contoured every 0.75 K) during day −1. All the zero contours are omitted.

values at day −1 in the upper troposphere, reaching 180 m. A progressive eastward increase of the altitude of the maximum amplitude from 300 hPa over the Pacific Ocean to 200–150 hPa over the Atlantic Ocean is evident, and may be suggesting upward energy dispersion (Lim and Wallace 1991). In addition, the vertical structure displays the typical westward tilt with height of the baroclinic waves, which is more pronounced from the surface to 300 hPa, and less from 250 hPa and above. The v' vertical distribution (Fig. 8(d)) resembles that of z' (Fig. 8(a)), with maximum values reaching up to -18 m s^{-1} over 90°W.

Temperature perturbations (Fig. 8(b)) are maximum at the mid troposphere (around 600–500 hPa) and also over the lower stratosphere (~200 hPa). Typical perturbation absolute values reach 3 to 4 K over the mid troposphere, while they are lower (up to 3 K) in the lower stratosphere. The change in sign of the temperature perturbation near 250 hPa is indicative of the position of the tropopause. The comparison of Fig. 8(a) and (b) show the characteristic baroclinic wave pattern of warm (cold) highs (lows) in the troposphere and warm (cold) lows (highs) in the stratosphere. In addition, the temperature perturbation field displays an eastward tilt with height, while geopotential height perturbations are tilted to the west (Fig. 8(a)). This structure distinguishes developing baroclinic waves, as it produces poleward heat fluxes favourable for eddy energy generation by baroclinic conversions. In this sense, maximum poleward heat fluxes are found between the geopotential height centres in the middle troposphere and those with reverse sign in the lower stratosphere (Fig. 8(f)). Due to the westward tilt of the wave, intense poleward heat fluxes in the stratosphere are placed about 15° west of the corresponding fluxes in the troposphere.

The vertical velocity perturbation field (Fig. 8(c)) exhibits a coherent vertical structure over the troposphere and lower stratosphere, with maximum values of about 0.08 Pa s^{-1} in the 500–600 hPa layer. Such a distribution is consistent with the divergence perturbation field (not shown), where upward (downward) motion eastward of the trough (ridge) is related to maximum convergence (divergence) at lower levels and maximum divergence (convergence) in the lower stratosphere. Upward heat fluxes are found in the middle troposphere (Fig. 8(e)) thus favouring eddy available potential energy conversion to eddy kinetic energy. Conversely, above the tropopause, Fig. 8(c), (d) and (e) suggests that, as cold air ascends and warm air descends, local kinetic energy

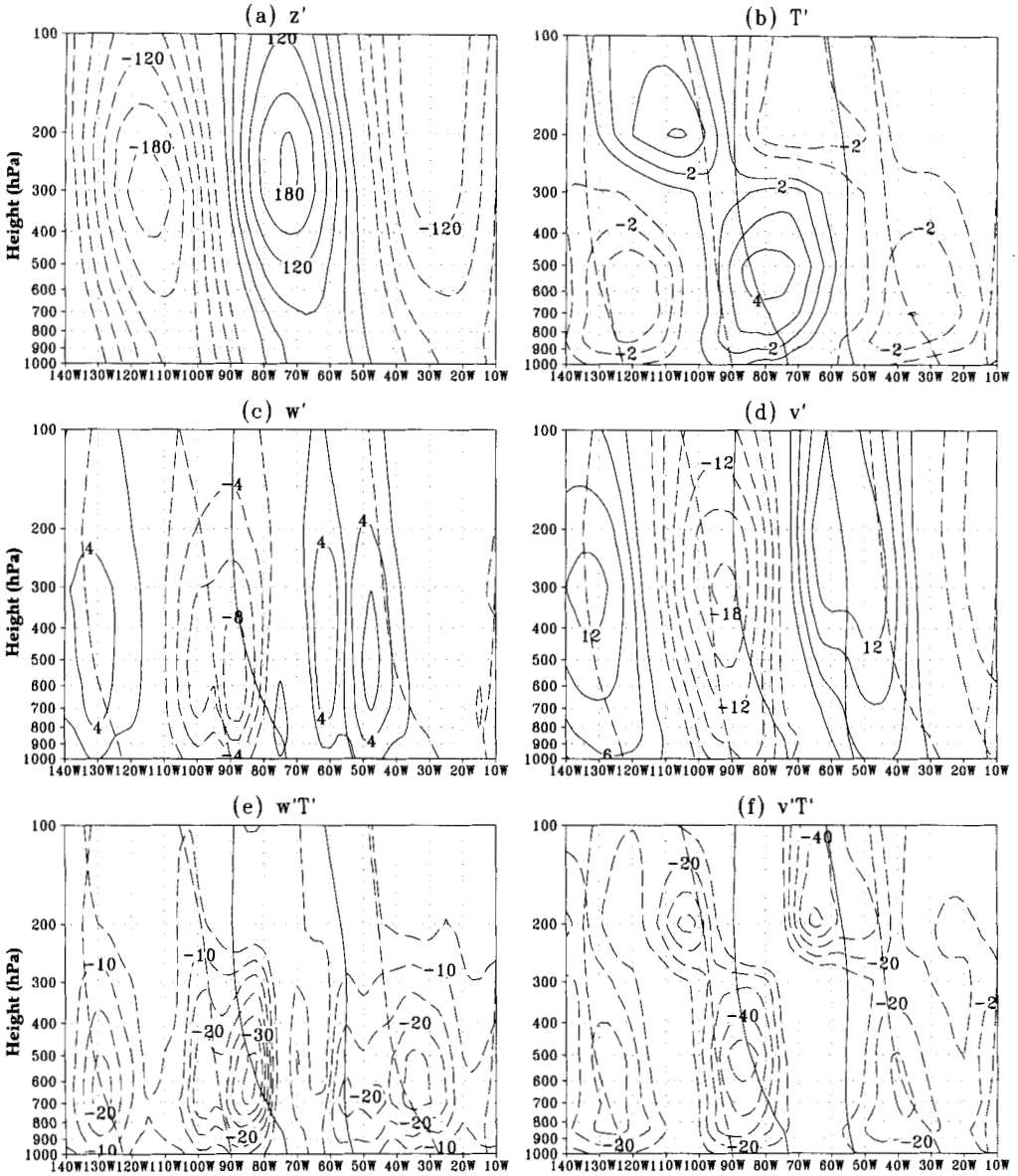

Figure 8. Longitude–height sections of negative composites of: (a) geopotential height perturbation, (b) temperature perturbation, (c) vertical velocity perturbation, (d) merididonal wind perturbation, (e) vertical heat flux and (f) poleward heat flux, averaged over 50–55°S during day −1. Contour intervals are: (a) 30 m, (b) 1 K, (c) 2×10^{-2} Pa s^{-1}, (d) 3 m s^{-1}, (e) 5×10^{-2} Pa s^{-1}, and (f) 10 m s^{-1}. From (b) to (f) both the −60 m and the 60 m geopotential height perturbation contours are shown for reference (thick dashed and solid lines respectively). The zero contours are omitted.

is being converted to potential energy, which is consistent with the evidence that these waves maximize near the tropopause (Wallace and Hobbs 1977).

Hence, our results show that subpolar synoptic-scale waves determine daily ozone patterns due to dynamical advective processes. This is possible due to the equivalent-barotropic vertical structure of the waves, which attain greatest amplitudes very close to the level where ozone partial pressure also reaches a maximum.

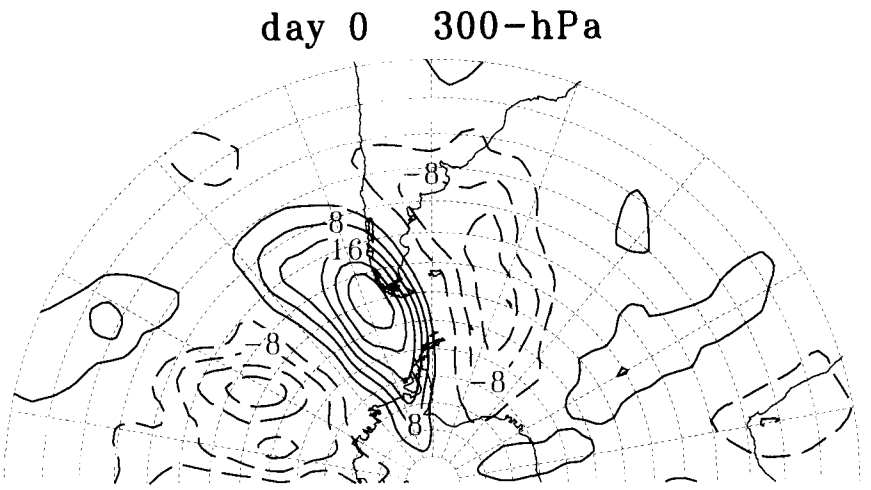

Figure 9. As Fig. 5 but for the subpolar mode positive composites. Only day 0 is displayed.

(*c*) *Positive composites*

Figure 9 shows the positive composites for the 300 hPa meridional wind perturbations on day 0. This wave pattern corresponds well (in opposite sign) with the negative composites (Fig. 5(b)), although some differences are discernible. In this case, the two centres over the southern Pacific Ocean are more intense than their negative-composite counterparts, reaching values of about -16 m s^{-1} for the centre over 120°W and 24 m s^{-1} for the one near SSA. Conversely, over the Atlantic Ocean, the positive-composite field displays weakest and noisy centres.

Both negative- and positive-composite sets display waves with similar length (~5000 km), although the positive set comprises slightly slower waves. As a consequence, the negative-composite cyclone advances more slowly over SSA than its anticyclonic counterpart (Fig. 5(c)).

Total ozone and upper-level positive-composite circulation fields for day 0 (that is the time when the ozone perturbation reaches a maximum over SSA (Fig. 10)) show that low-ozone content (~280 DU) is related to an anticyclonic system over the south-eastern Pacific Ocean; while a relative maximum of ozone (~340 DU) is seen over SSA in association with the local cyclonic system. In addition, both lower-stratospheric z' and T' fields are found to be highly correlated with the corresponding ozone perturbation field (not shown) yielding similar ratios of ozone perturbations to z' and T' as those of the negative composite set (Fig. 7). Moreover, despite the sign of the composite, over the south-eastern Pacific sector ozone perturbation values are larger (about 30 DU) than those over SSA, which do not exceed 25 DU. This may be due to the relative zonal differences in the background mean ozone content (Fig. 1(a)). The same behaviour is also noted for the geopotential height perturbation fields, whereas stronger systems are typically found west of SSA.

The vertical structure of the positive-composite perturbations is similar to that described for the negative composites (not shown), thus resembling the typical structure of baroclinic mid- to high-latitude waves. Positive-composite patterns also show that subpolar mode baroclinic disturbances are responsible for large total ozone fluctuations by means of dynamical mechanisms, as ozone mixing ratio is conserved for time-scales less than ten days or so.

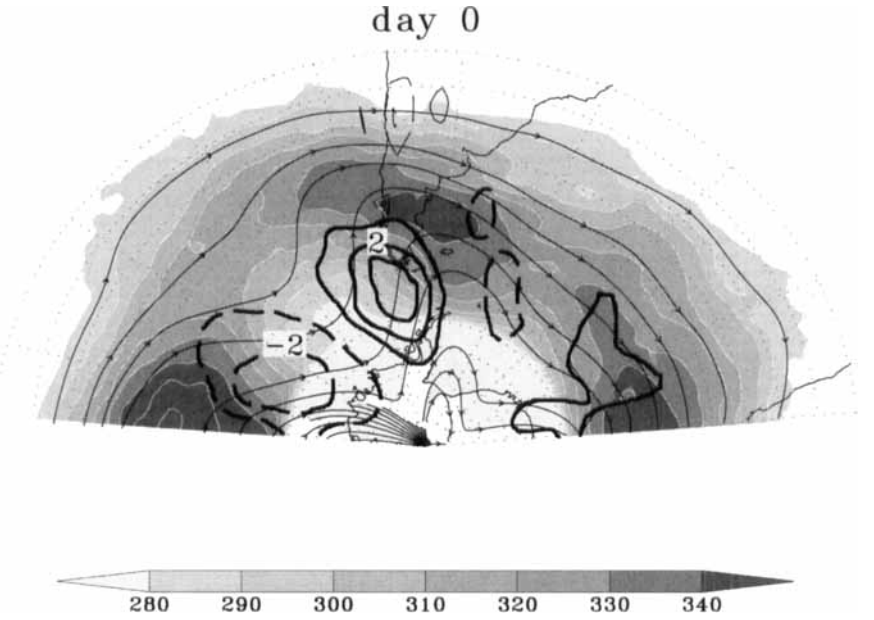

Figure 10. Positive composites of total ozone for day 0 (shaded every 10 DU), streamlines at 300 hPa (thin contours), and 100 hPa vertical velocity field (thick contoured every 1×10^{-2} Pa s^{-1}), with zero contours omitted.

6. Conclusions

In this paper, SH winter mid- to high-latitude atmospheric fields and total ozone distributions were examined. Zonal asymmetries of mean ozone display a clear wave number one pattern at middle and high latitudes with a minimum over SSA. It is suggested that this pattern is the result of the combined action of horizontal and vertical advection by planetary waves (in agreement with other authors) and of non-conservative ozone anomaly net source. Nevertheless, quantitative estimations of those terms need to be performed to address the relative importance of each of the processes involved.

SH winter transient circulation and ozone variations were also examined. A strong correspondence was found between the standard deviation of daily departures from seasonal means (after removing seasonal and interannual variability) of both upper-troposphere geopotential height and total ozone fields; this confirms the primary role of atmospheric fluctuations in driving ozone variations. In particular, higher-frequency ozone-track regions coincide with storm-track locations, as inferred from the standard deviations of filtered geopotential height and ozone perturbations. Moreover, it was shown that the ozone track attains its maximum over the southern Indian Ocean slightly downstream of the storm-track maximum. Conversely, over the southern Pacific basin, both ozone and storm track display minimum values while the standard deviations of unfiltered geopotential and ozone are maxima. This result indicates that ozone fluctuations over that region are probably due to intermediate-frequency atmospheric variability such as blocking events.

The synoptic-scale atmospheric fluctuations and related ozone signatures were studied over SSA, where the climatological winter total ozone field displays a minimum, and both the ozone and storm track have relative maximum values. A REEOFs analysis, applied to the meridional-wind perturbation at 300 hPa, was chosen as the most suitable method for identifying propagating waves that maximize at preferred geographical

locations. The leading winter mode over SSA is associated with a wave train travelling eastward at subpolar latitudes (referred to as a subpolar mode). The wave train follows a mainly zonal path over the south-eastern Pacific Ocean and SSA, whereas in the south-western Atlantic, it detours equatorwards while the waves become more meridionally elongated in the north-west to south-east direction. Wavelengths are of about 5000 km, which corresponds to wave number 4–5 over these latitudes.

Composite fields of negative (positive) sign of the main atmospheric variables and ozone were constructed, by averaging the situations when subpolar mode temporal coefficients are lower (higher) than a predefined threshold. Negative composites are associated with an upper-tropospheric anticyclonic disturbance evolving over SSA. This in turn is responsible for a transient depression in the total ozone field, by means of both horizontal and vertical advection, as the ozone mixing ratio is conserved for time-scales of a few days. Moreover, inspection of lower-stratospheric temperature and geopotential height perturbations, and of ozone perturbations, reveals that the sensitivity ratios of ozone to changes in the lower-stratospheric variables correspond to those expected solely by dynamical forcing. Waves associated with subpolar winter mode negative composites display the typical structure of baroclinic mid- to high-latitude waves, characterised by: (i) both v' and z' maxima are located at the upper troposphere; (ii) a vertical distribution of T' with a double-structure maximum located in the middle troposphere and lower stratosphere, respectively; (iii) a horizontal structure of v' that is meridionally elongated throughout the troposphere and lower stratosphere; (iv) an eastward tilt with a high of T' to the west of z', that favours the perturbation growth by baroclinic conversions.

The subpolar mode positive composites are associated with the passage of a cyclone over SSA, which drives a corresponding maximum signature in the total ozone field. Overall, the positive-composite set resembles much of the characteristics of the negative set, although the positive composites are associated with rather slower waves (8–7 m s^{-1}) in contrast to the slightly faster negative subpolar mode waves (9–8 m s^{-1}).

In conclusion, we found that the main synoptic-scale variability mode over SSA is intimately linked to daily ozone fluctuations over the region. Moreover, we have shown that subpolar baroclinic waves control ozone changes by dynamical advective processes. The essence of ozone variations due to subpolar baroclinic waves can be generalized using the following conceptual model, and with the aid of Fig. 6.

During the life cycle of a baroclinic wave, the tropopause is modulated and is typically elevated over the ridge and depressed over the trough. As the baroclinic wave reaches maximum amplitude in the upper troposphere and dies away in the lower stratosphere, the ozone layer is deeper where the tropopause is lower and vice versa. Due to the fact that air motion in the lower stratosphere is nearly isentropic, it tends to follow the tropopause. Hence ascent (descent) and south-eastward (north-eastward) motions are expected at the rear of the ridge (trough). This leads to the ozone column content lowering over the upper-tropospheric high-pressure areas, whereas ozone is found to accumulate over the upper-tropospheric low-pressure regions.

ACKNOWLEDGEMENTS

The authors thank Dr W. Randel and the anonymous reviewers for their comments and suggestions that helped to improve substantially the original manuscript. Also we are grateful to Dr R. McPeters and NASA TOMS Processing Team for providing TOMS and SBUV data. The present work was partially supported by UBA Grants JX01 and JX80 and also by PICT 07-03781 Grant.

REFERENCES

Allen, D. R. and Reck, R. A. 1997 Daily variations in TOMS total ozone data. *J. Geophys. Res.*, **102,** 13603–13608

Ambrizzi, T., Kayano, M. T. and Stephenson, D. B. 1998 A comparison of global tropospheric teleconnections using observed satellite and general circulation model total ozone column data for 1979–91. *Clim. Dyn.*, **2,** 133–150

Andrews, D. G., Holton, J. R. and Leovy, C. B. 1987 *Middle Atmosphere Dynamics*. Academic Press, New York, USA

Berbery, H. and Vera, C. 1996 Characteristics of the southern hemisphere winter storm track with filtered and unfiltered data. *J. Atmos. Sci.*, **53,** 468–481

Blackmon, M. L., Lee, Y.-H. and Wallace, J. M. 1984 Horizontal structure of 500 mb height fluctuations with long, intermediate and short time scales. *J. Atmos. Sci.*, **41,** 961–979

Fisher, M. A., O'Neill, A. and Sutton, R. 1993 Rapid descent of mesospheric air into the stratospheric polar vortex. *Geophys. Res. Lett.*, **20,** 1267–1270

Hood, L. L., McCormack, J. P. and Labitzke, K. 1997 An investigation of dynamical contributions to midlatitude ozone trends in winter. *J. Geophys. Res.*, **102,** 13079–13093

Kurzeja, R. J. 1984 Spatial variability of total ozone at high latitudes in winter. *J. Atmos. Sci.*, **41,** 695–697

Lau, K.-H. and Chan, P. H. 1985 Aspects of the 40–50 day oscillation during the northern winter as inferred from outgoing longwave radiation. *Mon. Weather Rev.*, **113,** 1889–1909

Lim, G.-H. and Wallace, J. M. 1991 Structure and evolution of baroclinic waves as inferred from regression analysis. *J. Atmos. Sci.*, **48,** 1718–1731

McKenna, D. S., Jones, R. L., Austin, J. E., Browell, V., McCormick, M. P., Krueger, A. J. and Tuck, A. F. 1989 Diagnostic studies of the Antarctic vortex during the 1987 airborne Antarctic ozone experiment: Ozone miniholes. *J. Geophys. Res.*, **94,** 11641–11668

McPeters, R. D. and Beach, E. 1996 'TOMS Nimbus-7 and Meteor-3, version 7'. NASA/GSFC, Greenbelt, Maryland, USA

McPeters, R. D., Milles, T., Flynn, L. E., Wellemeyer, C. G. and Zawodny, J. M. 1994 Comparison of SBUV and SAGE II ozone profiles: Implications for ozone trends. *J. Geophys. Res.*, **99,** 20513–20524

Mote, P. W., Holton, J. R. and Wallace, J. M. 1991 Variability in total ozone associated with baroclinic waves. *J. Atmos. Sci.*, **48,** 1900–1903

Newman, P. A. and Randel, W. J. 1988 Coherent ozone–dynamical changes during the southern hemisphere spring, 1979–1986. *J. Geophys. Res.*, **93,** 12585–12606

O'Lenic, A. and Livesey, M. 1988 Practical considerations in the use of rotated principal component analysis (RPCA) in diagnostic studies of upper-air height fields. *Mon. Weather Rev.*, **116,** 1682–1689

Orlanski, I., Marino, M., Menendez, C. and Katzfey, J. 1989 'The role of cyclones in the daily variability of antarctic ozone'. Pp. 144–147 of Preprints of the third international conference on southern hemisphere meteorology and oceanography, Buenos Aires, Argentina. American Meteorological Society, Boston, USA

Orsolini, Y., Cariolle, D. and Dèque, M. 1995 Ridge formation in the lower stratosphere and its influence on ozone transport: A general circulation model study during late January 1992. *J. Geophys. Res.*, **100,** 11113–11135

Orsolini, Y. J., Stephenson, D. B. and Doblas-Reyes, F. J. 1998 Storm track signature in total ozone during northern hemisphere winter. *Geophys. Res. Lett.*, **25,** 2413–2416

Randel, W. J. 1992 'Global atmospheric circulation statistics, 1000–1 mb'. NCAR Technical Note 366+STR, National Center for Atmospheric Research, Boulder, Colorado, USA

Randel, W. J. and Cobb, J. B. 1994 Coherent variations of monthly mean total ozone and lower stratospheric temperature. *J. Geophys. Res.*, **99,** 5433–5447

Randel, W. J. and Newman, P. 1998 The stratosphere in the southern hemisphere. Pp. 243–282 in *Meteorology of the southern hemisphere*. Eds. D. J. Karoly and D. G. Vincent. American Meteorological Society, Boston, USA

Randel, W. J. and Wu, F. 1995 'Climatology of stratospheric ozone based on SBUV and SBUV/2 data: 1978–1994'. NCAR Technical Note 412+STR, National Center for Atmospheric Research, Boulder, Colorado, USA

Reed, R. J. 1950 The role of vertical motions in ozone–weather relationships. *J. Meteorol.*, **7,** 263–267

Rood, R. B., Nielsen, J. E., Stolarski, R. S., Douglass, A. R., Kaye, J. A. and Allen, D. J. 1992 Episodic total ozone minima and associated effects on heterogeneous chemistry and lower stratospheric transport. *J. Geophys. Res.*, **97,** 7979–7996

Salby, M. L. and Callaghan, P. F. 1993 Fluctuations of total ozone and their relationship to stratospheric air motions. *J. Geophys. Res.*, **98,** 2715–2727

Schoeberl, M. and Krueger, A. 1983 Medium scale disturbances in total ozone during southern hemisphere summer. *Bull. Am. Meteorol. Soc.*, **64,** 1358–1365

Schubert, S. D. and Munteanu, M.-J. 1988 An analysis of tropopause pressure and total ozone correlations. *Mon. Weather Rev.*, **116,** 569–582

Sheperd, T. 1997 The influence of dynamical processes on ozone abundance. In *Ozone Science: A Canadian perspective on the changing ozone layer*. Eds. D. I. Wardle, J. B. Kerr, C. T. McElroy and D. R. Francis. Environment Canada, University of Toronto, Toronto, Canada

Solomon, S. and Garcia, R. R. 1985 Transport processes and ozone perturbations. *J. Geophys. Res.*, **90,** 12981–12989

Stanford, J. L., Ziemke, J. R., McPeters, R. D., Krueger, A. J. and Barthia, P. K. 1995 'Spectral analyses, climatology and inter-annual variability of Nimbus-7 TOMS version of 6 total column ozone'. Technical Report 1360, NASA, Greenbelt, Maryland, USA

Stephenson, D. B. and Royer, J.-F. 1995 Low frequency variability of total ozone mapping spectrometer and general circulation model total ozone stationary waves associated with the El Niño/Southern Oscillation for the period 1979–1988. *J. Geophys. Res.*, **100,** 7337–7346

Trenberth, K. E. 1991 Storm tracks in the southern hemisphere. *J. Atmos. Sci.*, **48,** 2159–2178

1992 'Global analyses from ECMWF and atlas of 1000 to 10 mb circulation statistics'. NCAR Technical Note NCAR/TN–373+STR. National Center for Atmospheric Research, Boulder, Colorado, USA

Vaughan, G. and Price, J. D. 1991 On the relationship between total ozone and meteorology. *Q. J. R. Meteorol. Soc.*, **117,** 1281–1298

Vera, C. S. and Vigliarolo, P. K. 2000 A diagnostic study of cold-air outbreaks over South America. *Mon. Weather Rev.*, **128,** 3–24

Wallace, J. M. and Hobbs, P. V. 1977 *Atmospheric science: An introductory survey*. Academic Press, New York, USA

Wirth, V. 1993 Quasi-stationary planetary waves in total ozone and their correlation with lower stratospheric temperature. *J. Geophys. Res.*, **98,** 8873–8882

Ziemke, J. R., Chandra, S., McPeters, R. D. and Newman, P. A. 1997 Dynamical proxies of column ozone with applications to global trend models. *J. Geophys. Res.*, **102,** 6117–6129